Going beyond the classical amphiphilicity paradigm: Self-assembly of completely hydrophobic polymers into free-standing sheets and hollow nanostructures in solvents of variable quality

Huanting Huang,[a] Yin Liao,[a] Weifeng Bu,*[a] Wenjie Wang[b] and Jing Zhi Sun*[b]

[a]Key Laboratory of Nonferrous Metals Chemistry and Resources Utilization of Gansu Province, State Key Laboratory of Applied Organic Chemistry, and College of Chemistry and Chemical Engineering, Lanzhou University, Lanzhou, Gansu, 730000, China, Email: buwf@lzu.edu.cn

[b]MOE Key Laboratory of Macromolecular Synthesis and Functionalization, Department of Polymer Science and Engineering, Zhejiang University, Hangzhou, Zhejiang, 310027, China, Email: sunjz@zju.edu.cn

Experimental

Materials and instruments. PS-1, PS-2, P3HT-1 and P3HT-2 were purchased from Polymer Source Inc. and used without further purification. PPA-1,[29,30] PPA-2,[29,30] and SVP-6[19] (polyoxometalate-based nanocomposite) were synthesized according to the procedures described in the literatures, respectively. UV-vis absorption spectra were recorded by using a Shimadzu 2550 spectrophotometer. X-ray diffraction was carried out on a PHILIPS X'Pert Pro diffractometer using Cu Kα radiation at a wavelength of 1.5416 Å. The TEM and SEM images were achieved by operating a JEM-2100 at 200 kV and a field emission Hitachi S-4800, respectively. The SEM measurement required depositing a 4-nm thick gold layer on the surface of the sample by using Hitachi E-1045 ion sputter. The resulting conductive surface resulted in the absence of electric charging that was usually generated during the process of SEM measurements and thus high quality SEM images was obtained. All measurements were carried out at 20 °C.

Dispersion preparation. PPA-2 was first dissolved in toluene at 20 °C. And then, methanol was added in one portion with a stirring speed of 1200 rpm, where the volume ratios were controlled at 25%, 33%, 43% 50%, 67%, 75%, and 90%, respecti ely. Finally, seven heavily opaque dispersions formed. Similarly, the dispersions were also prepared for PPA-1, PS-1, PS-2, P3HT-1 and P3HT-2. In all the cases, toluene and methanol are good and poor solvents of these completely hydrophobic polymers, respectively. The final concentrations of both PPA-1 and PPA-2 were controlled at 0.33 mg/mL. The others occupied a concentration of 0.10 mg/mL in the toluene/methanol mixture solvents with various methanol volume ratios. For the encapsulation experiments of hollow nanostructures, PPA-1 or PPA-2 was first mixed together with SVP-6 in toluene and then

methanol was added in one portion with a methanol volume ratio of 90%. Their concentrations were again controlled at 0.33 mg/mL. All of these dispersions were aged for 10 min and then cast (5 μL) on carbon-coated copper grids and/or copper grids coated with a porous polymer membrane for TEM and SEM observations. These dispersions were further aged for 10 d and 30 d for time dependent microscopic observations.

Additional discussion

(a) We also prepared the dispersions by layering methanol with a toluene solution of PPA-2 with methanol volume ratios of 50% and 90%. During this procedure, the methanol was added extremely slowly to the polymer solution. And still, the precipitates formed within 10 min. They were further cast onto carbon-coated copper grids for TEM observations. The resulting TEM images showed that the sheets and hollow nanostructures formed with almost the same sizes, respectively. These observations suggest that the rate of methanol addition did not influence the formation of nanostructures.

(b) Starlike polymers have topologically branched nanostructures and thus lower viscosities in solution and melt states in comparison to their linear analogs with the same molecular weights. Linear homopolymers are simplest, most common, and representative in all kinds of topologies of polymers. Linear and star homopolymers not only have totally different topological architecture, but also completely distinctive effective potentials for their inter- and intramolecular interactions between the segments (C. N. Likos, H. Löwen, M. Watzlawek, B. Abbas, O. Jucknischke, J. Allgaier and D. Richter, *Phys. Rev. Lett.*, 1998, **80**, 4450). This is why we further perform this study here and so many comparable studies are carried out between star and linear polymers. Both of them experienced the self-assembly in solvents of weakening quality into sheetlike and hollow nanostructures. However, the details are different as addressed in the text.

Because of the branched topology, the density of the repeating unit in the linear arms decreases with the radial distance from the core. Therefore, the grafted chains pack under the state of constraint and have to get stretched away from the core. Reasonably, these tethered chains should be anisotropic, leading to the presence of anisotropic van der Waals attractions and thus the contribution to the hollow nanostructures. This is in sharp contrast to the really coiled conformation of PS. Of difference is that PPA is semiflexible and has anisotropic origin.

(c) Furthermore, the quantitative changes in solvent quality were estimated according to the following equation: $\delta_{mix} = \delta_1 V_{s1} + \delta_2 V_{s2}$, where δ_{mix}, δ_1, and δ_2 were the solubility parameters of toluene/methanol mixture solvent, toluene, and methanol and V_{s1} and V_{s2} were the volume ratios of toluene and methanol, respectively (1. C. M. Hansen, *Solubility Parameters: A User's Handbook, Second Ed.*, CRC Press Taylor & Francis Group, Boca Raton, FL, 2007. 2. P. S. He, *Structures and Properties of Polymers − A New Version, Chapter 9*, Science Press: Beijing, 2009). The obtained values of δ_{mix} ranged from 21.08 to 28.55 $J^{1/2}/cm^{3/2}$ (Table S1). They were compared with the solubility parameter of PS (δ_{PS}) to quantitatively estimate its solubility in the mixture solvents. When the methanol volume ratios were 25% and 33%, the difference values of $|\delta_{mix} - \delta_{PS}|$ were smaller than 3.5, suggesting that polystyrene was soluble in the mixture solvents. However, they were larger than 3.5 when the methanol volume ratios increased to ≥ 43%, indicating the presence of precipitates in the solvent mixtures. These estimated results were totally consistent with the experimental observations of PS in the toluene/methanol mixtures: the transparent

solutions were obtained at the methanol volume ratios of 25% and 33% and the precipitates were observed at the methanol volume ratios of ≥ 43%. Of difference was that PPA and P3HT partially precipitated under the former solvent conditions due to their much more rigid backbones. Similarly, they precipitated completely under the latter solvent conditions.
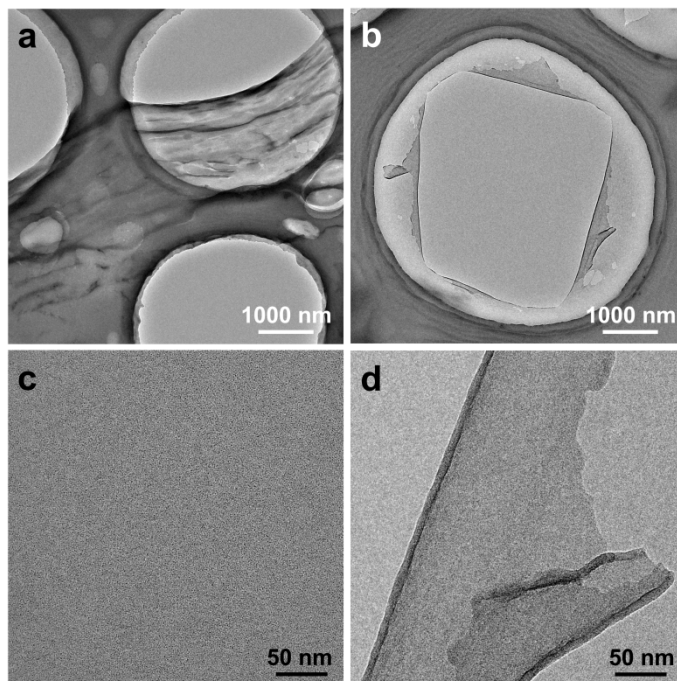

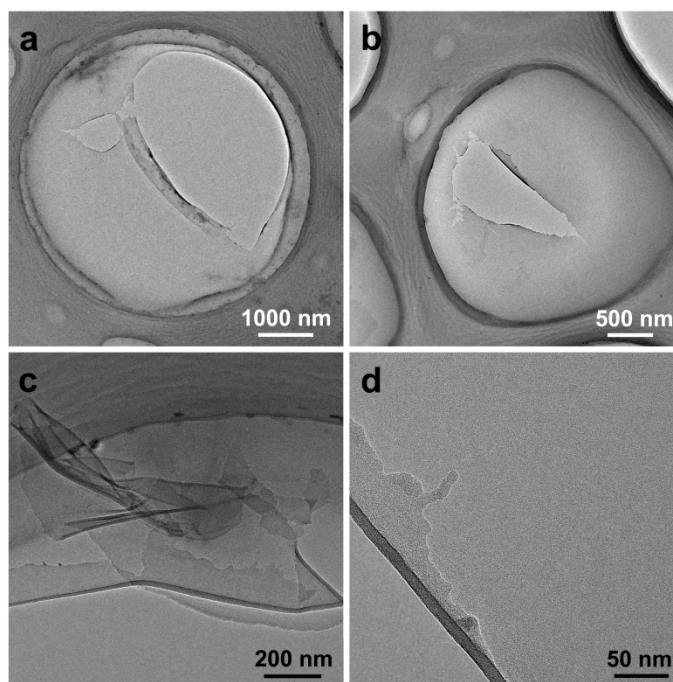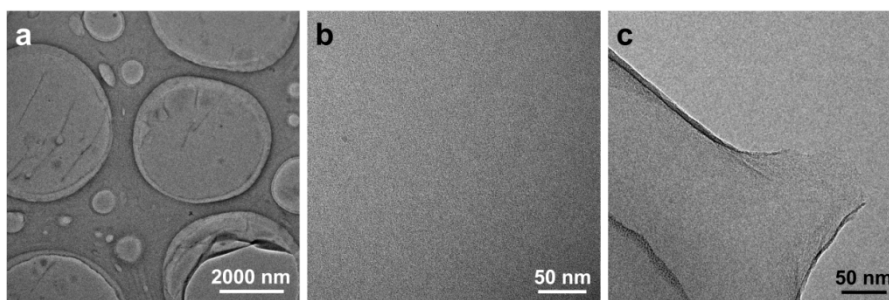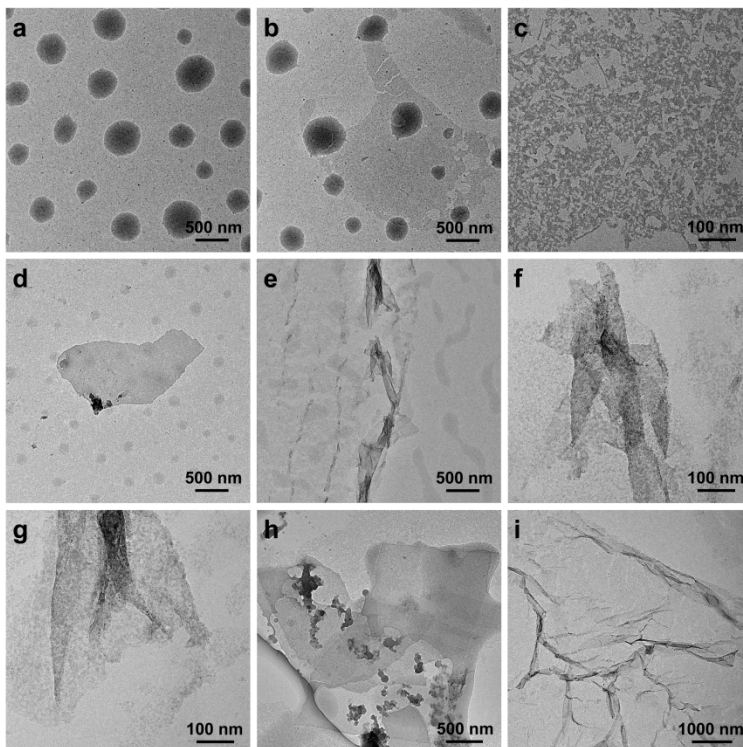**Fig. S1** TEM images of free-standing sheets of PPA-2 obtained from the toluene/methanol mixture solvent with a methanol volume ratio of 43%.

Fig. S2 TEM images of free-standing sheets of PPA-2 obtained from the toluene/methanol mixture solvent with a methanol volume ratio of 67%.

Fig. S3 TEM images of free-standing sheets of PPA-1 obtained from the toluene/methanol mixture solvent with a methanol volume ratio of 43%.
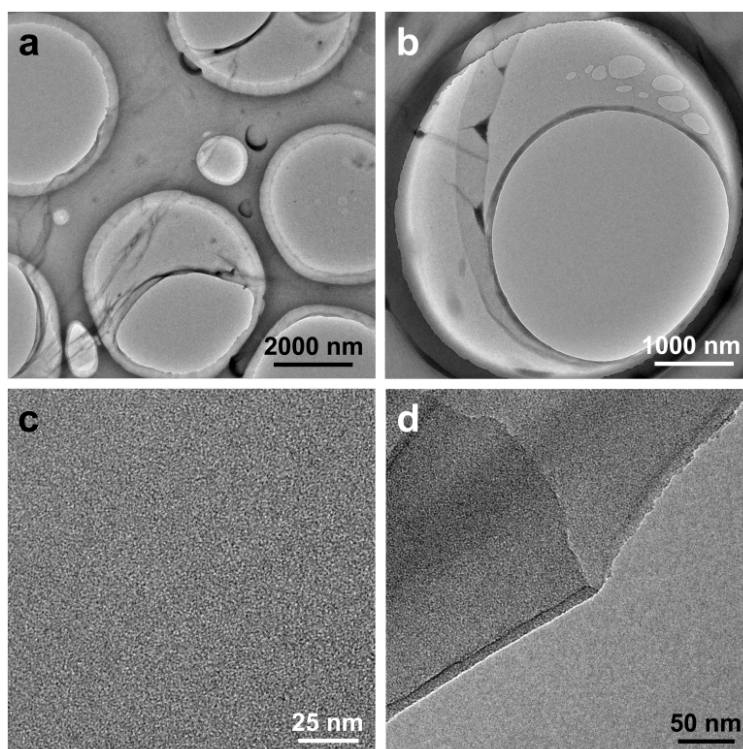
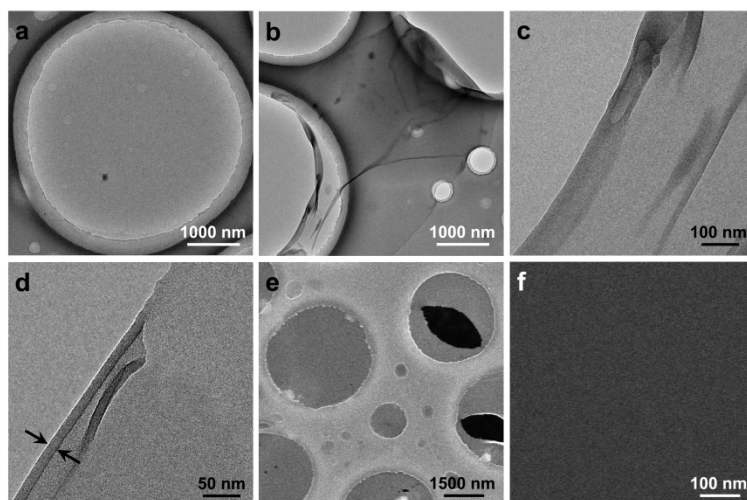**Fig. S4** TEM images of free-standing sheets of PPA-1 obtained from the toluene/methanol mixture solvent with a methanol volume ratio of 50%.
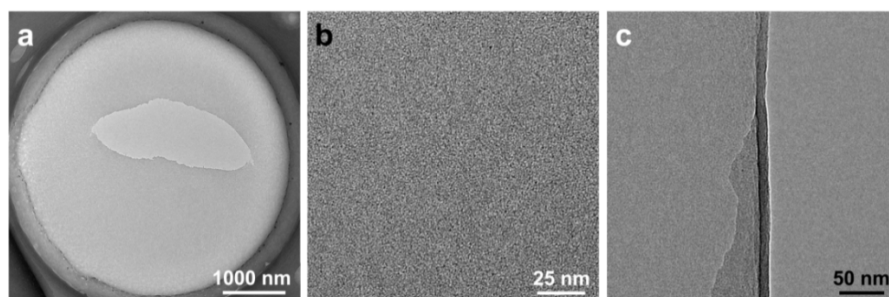
Fig. S5 TEM images of free-standing sheets of PPA-1 obtained from the toluene/methanol mixture solvent with a methanol volume ratio of 67%.
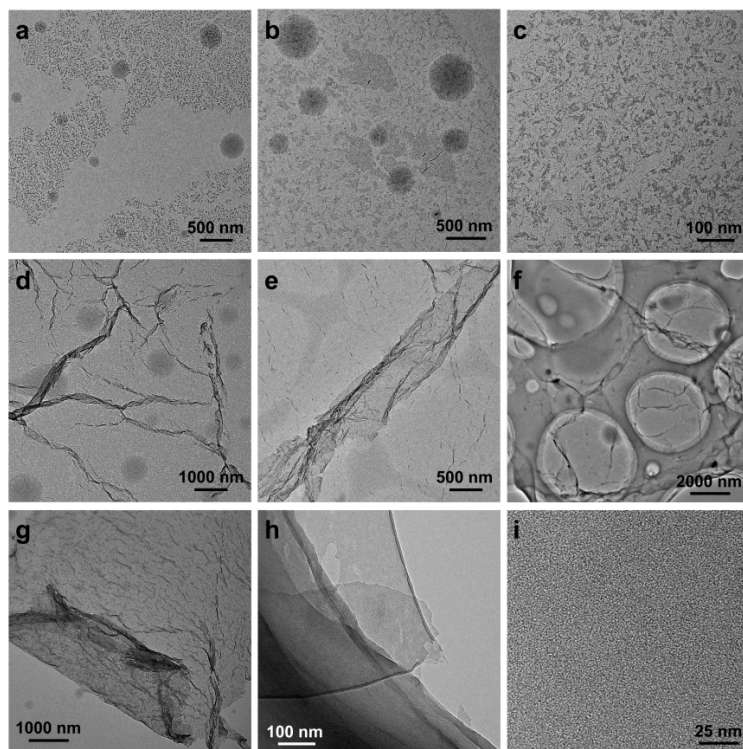
Fig. S6 TEM images of PPA-1 obtained from the toluene/methanol mixture solvent with a methanol volume ratio of 33%.

Fig. S7 TEM images of PPA-1 obtained from the toluene/methanol mixture solvent with a methanol volume ratio of 25%.

Fig. S8 TEM (a-d) and SEM images (e and f) of free-standing sheets of PS-1 obtained from the toluene/methanol mixture solvent with a methanol volume ratio of 50%.
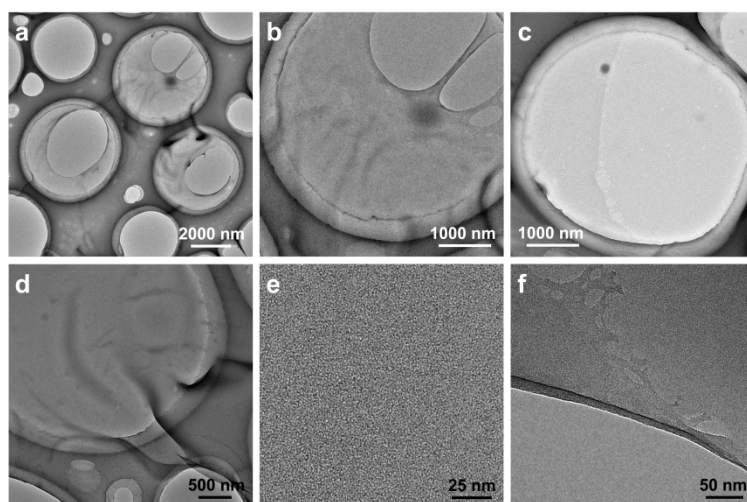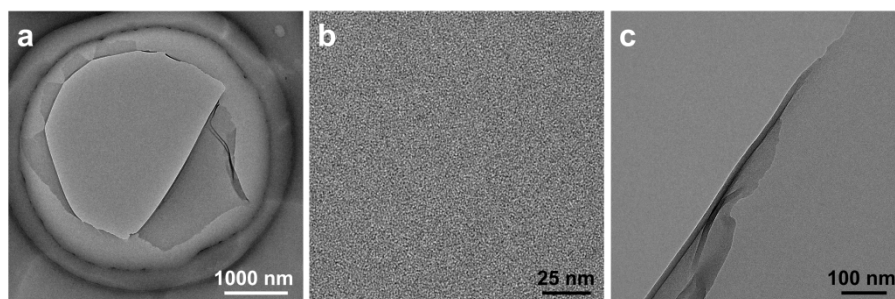

Fig. S9 TEM images of free-standing sheets of PS-1 obtained from the toluene/methanol mixture solvent with a methanol volume ratio of 43%.
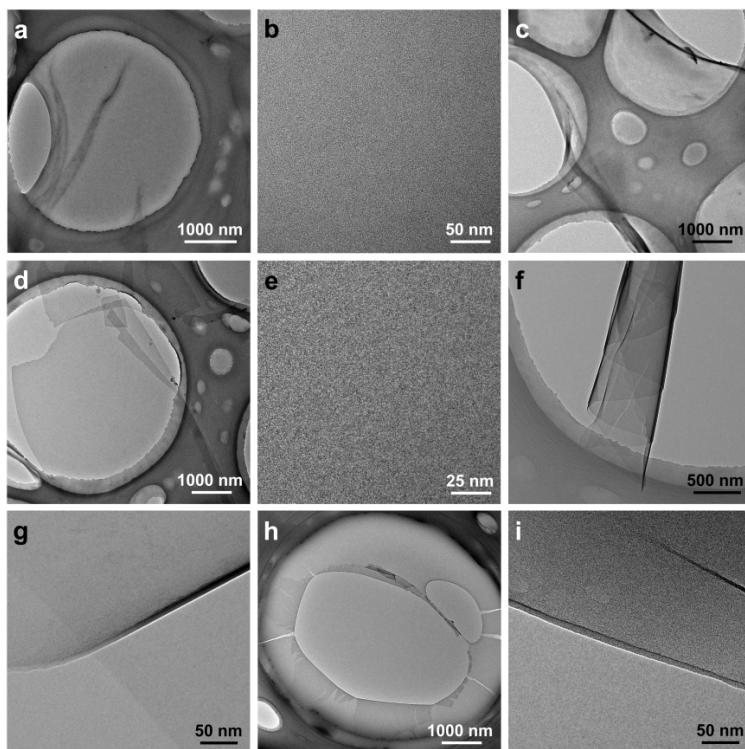

Fig. S10 TEM images of free-standing sheets of PS-1 obtained from the toluene/methanol mixture solvent with a methanol volume ratio of 67%.

Fig. S11 TEM images of free-standing sheets of PS-2 obtained from the toluene/methanol mixture solvent with methanol volume ratios of 43% (a and b), 50% (c-g), and 67% (h and i).
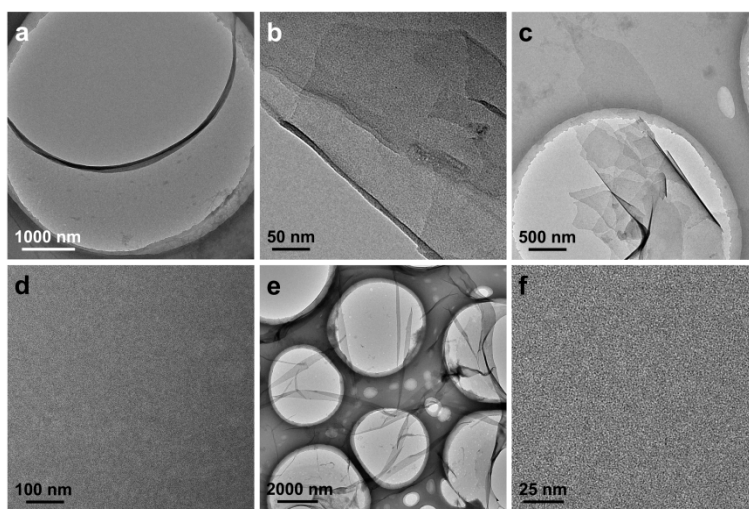

Fig. S12 TEM images of free-standing sheets of P3HT-1 obtained from the toluene/methanol mixture solvent with methanol volume ratios of 43% (a and b), 50% (c and d), and 67% (e and f).
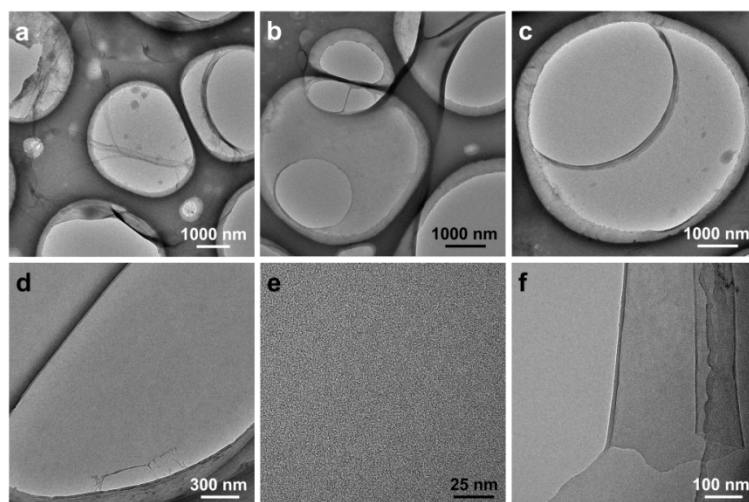
Fig. S13 TEM images of free-standing sheets of P3HT-2 obtained from the toluene/methanol mixture solvent with a methanol volume ratio of 33%.
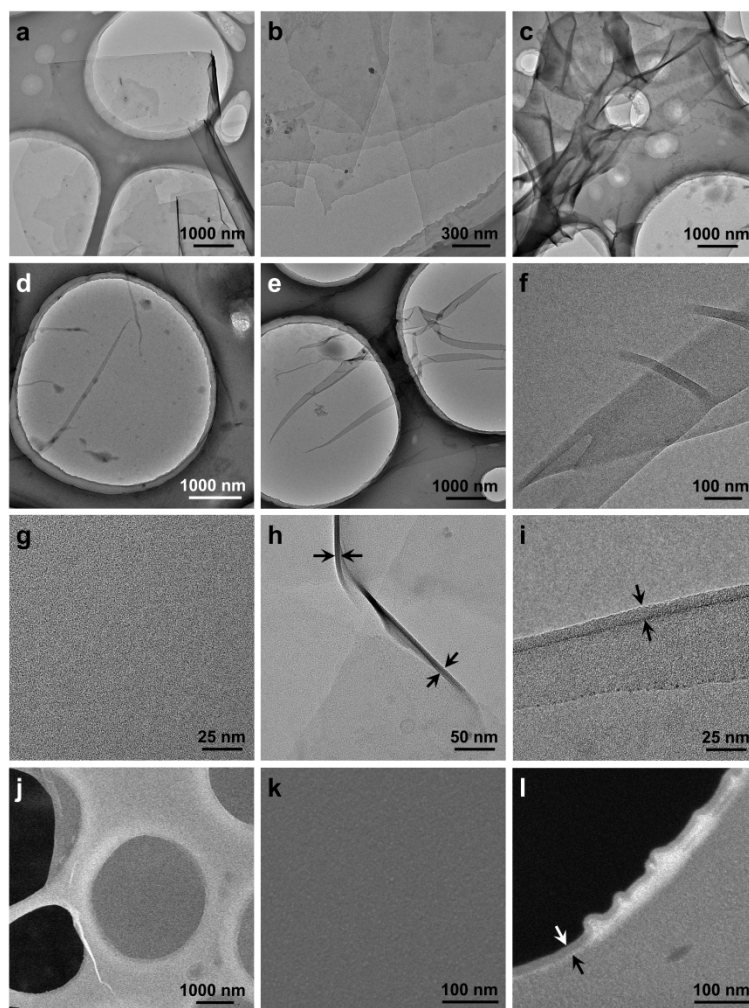

Fig. S14 TEM images of free-standing sheets of P3HT-2 obtained from the toluene/methanol mixture solvent with a methanol volume ratio of 50%.
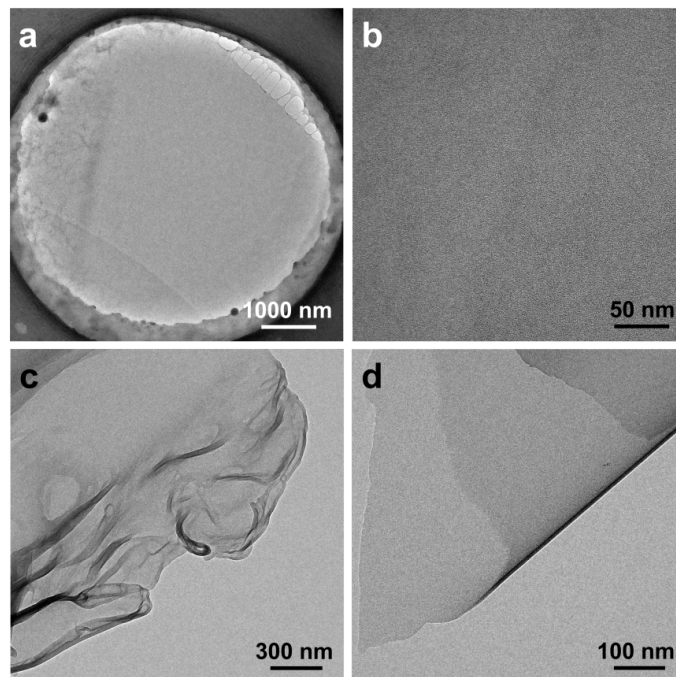
Fig. S15 TEM images of free-standing sheets of P3HT-2 obtained from the toluene/methanol mixture solvent with a methanol volume ratio of 67%.
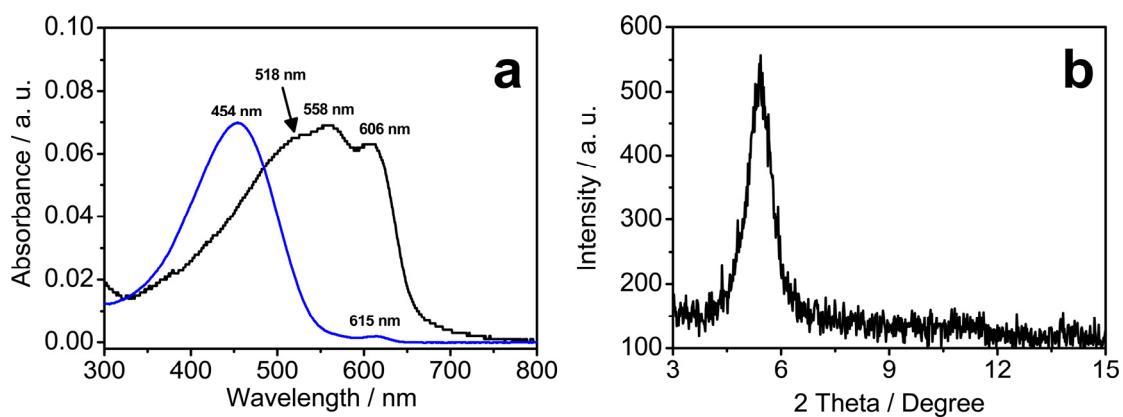

Fig. S16 (a) UV-vis spectra of the toluene solution (Blue line) and the sheet of P3HT-1 obtained in the toluene/methanol mixture solvent with a methanol volume of 50% (Black line). (b) X-ray diffraction pattern of the sheet of P3HT-1 obtained in the toluene/methanol mixture solvent with a methanol volume of 50%.
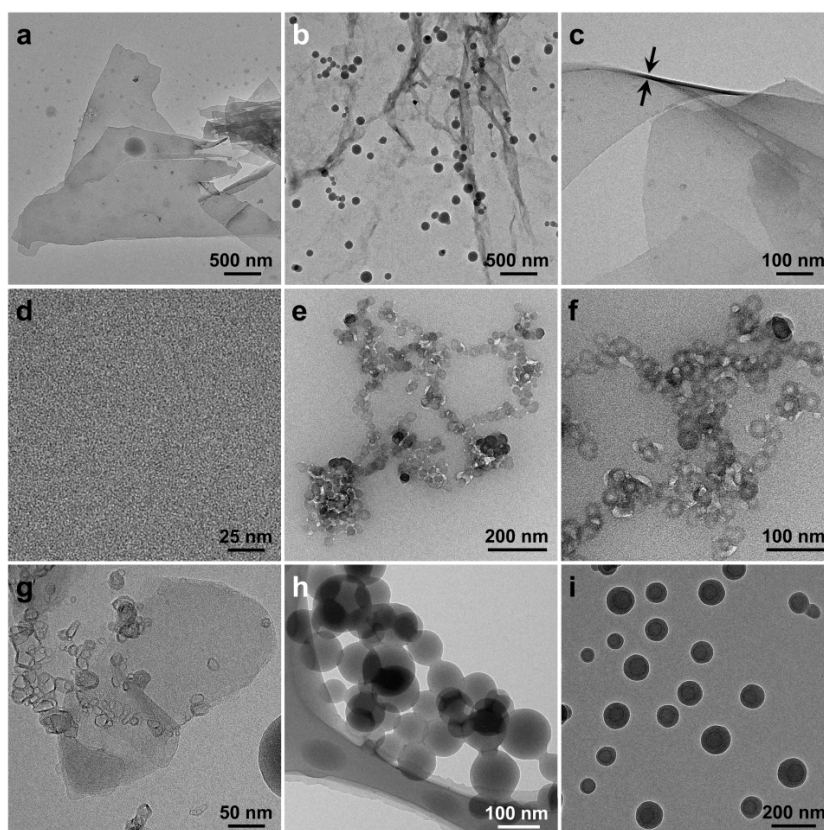
Fig. S17 TEM images of PPA-1 obtained from the toluene/methanol mixture solvent with a methanol volume ratio of 75%.
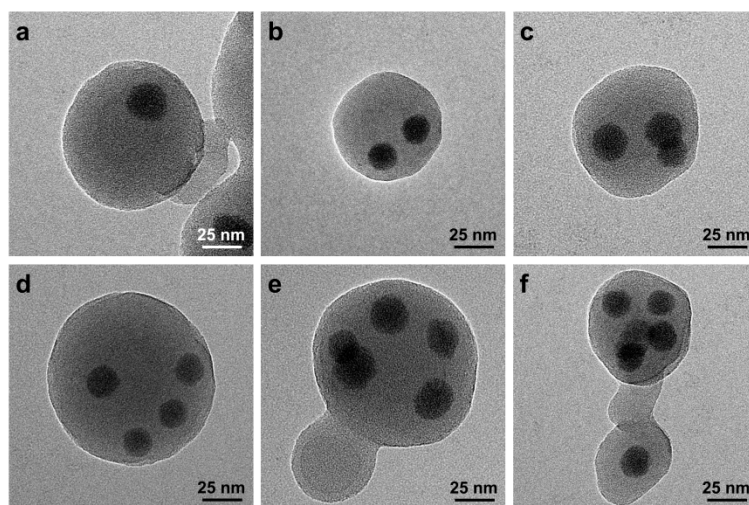

Fig. S18 TEM images of the mixture of PPA-2 and SVP-6 obtained from the toluene/methanol mixture solvent with a methanol volume ratio of 90%.
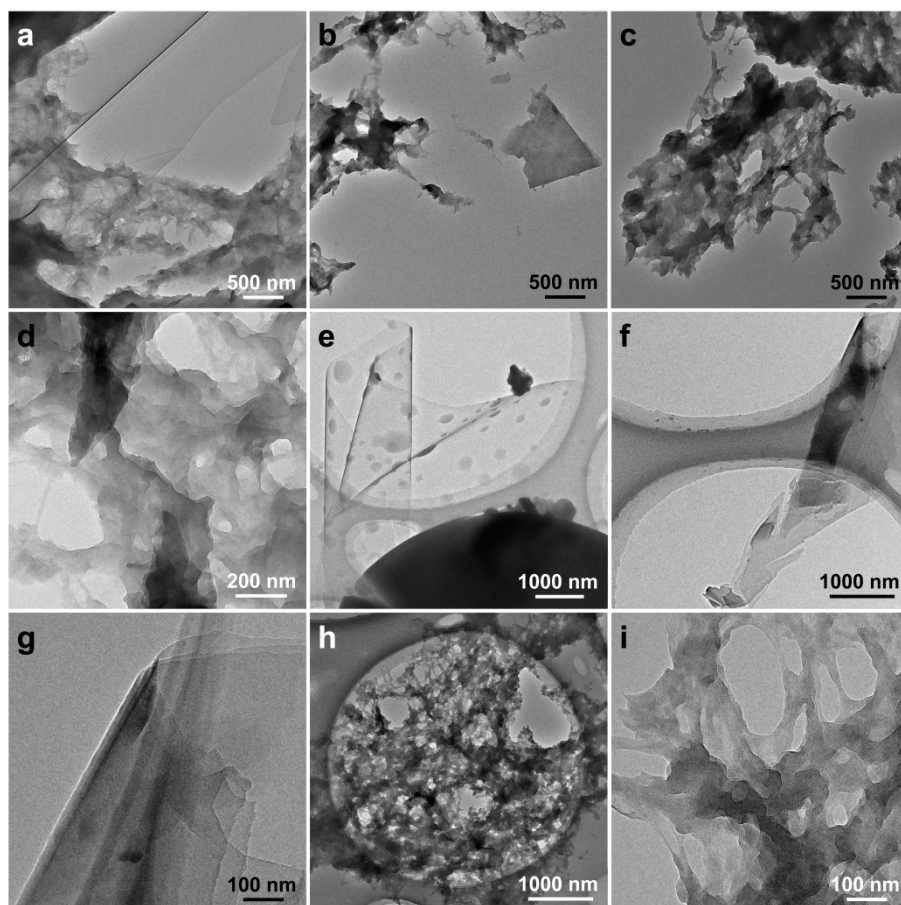
Fig. S19 TEM images of P3HT-1 obtained from the toluene/methanol mixture solvent with a methanol volume ratio of 75% (a-d) and 90% (e-i). Still, the sheets were highly uniform and occupied thicknesses of 8 ± 2 nm for both P3HT-1 and P3HT-2. Several irregular aggregates with a few tens of nanometers fused out from the sheet. Some of larger irregular aggregates were still held together with the free-standing sheets. And also, both the free-standing sheets and irregular aggregates were captured separately.
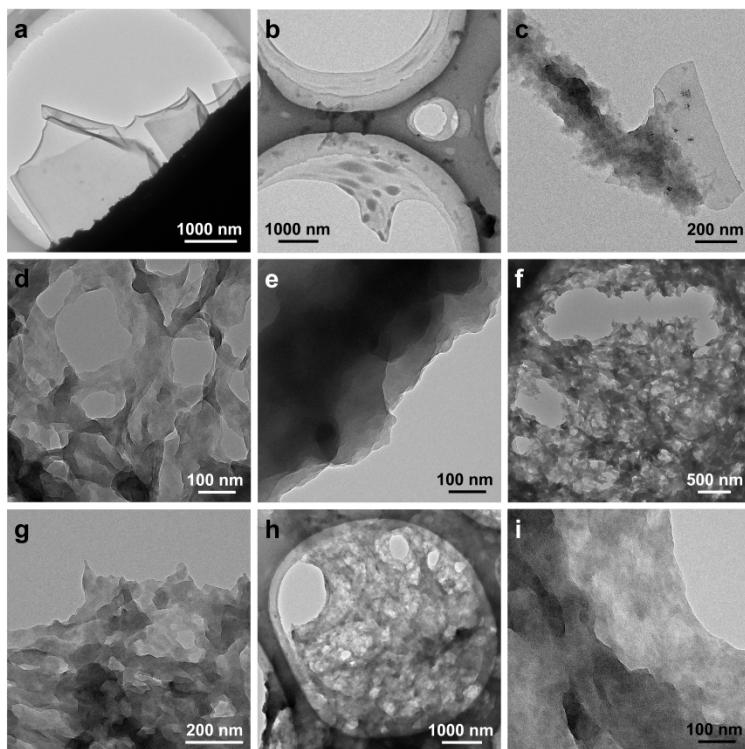
Fig. S20 TEM images of P3HT-2 obtained from the toluene/methanol mixture solvent with a methanol volume ratio of 75%.
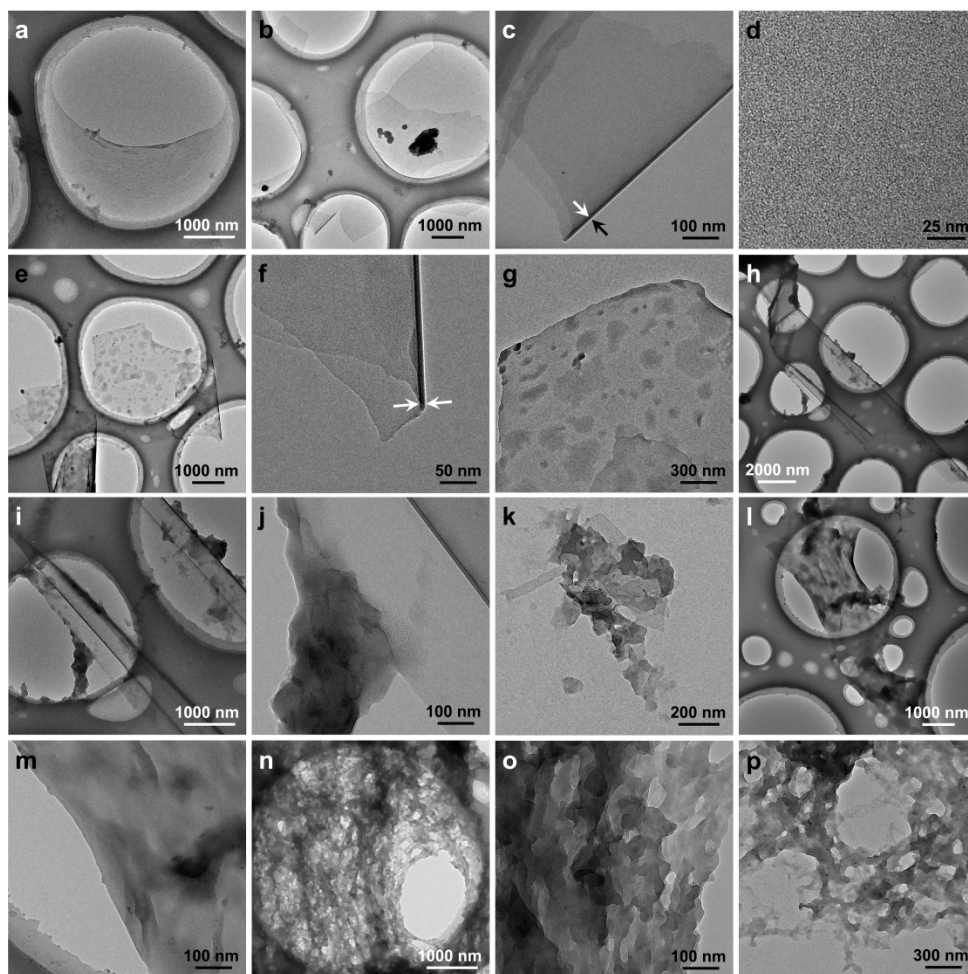
Fig. S21 TEM images of P3HT-2 obtained from the toluene/methanol mixture solvent with a methanol volume ratio of 90%.
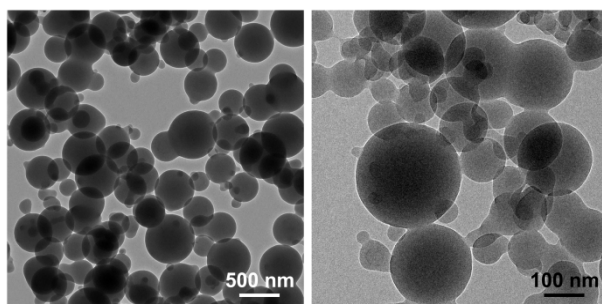

Fig. S22 TEM images of PS-1 (a) and PS-2 (b) obtained from the toluene/methanol mixture solvent with a methanol volume ratio of 90%. The collapsed and ruptured features and darker fringes were not observed in these spherical nanostructures, indicating that they were not hollow but rather solid in nature.
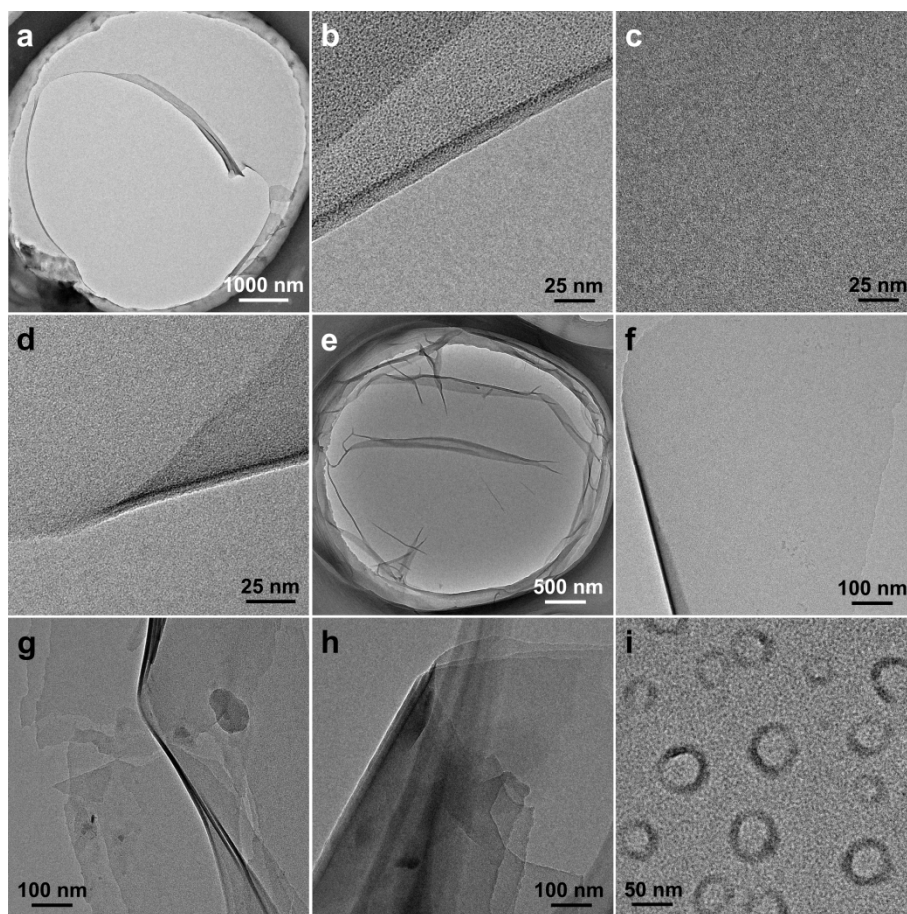
Fig. S23 TEM images of PPA-2 (a-c) and PPA-1 (d) were obtained from the toluene/methanol mixture solvent with a methanol volume ratio of 50% at the time of 30 d. TEM images of P3HT-2 were obtained from the toluene/methanol mixture solvent with a methanol volume ratio of 50% (e-h) at the time of 10 d. TEM image of PPA-2 obtained from the toluene/methanol mixture solvent with a methanol volume ratio of 90% at the time of 30 d (i).
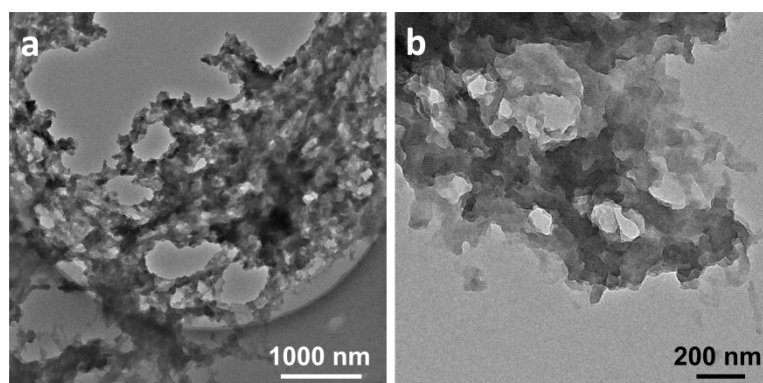

Fig. S24 Partial TEM images of P3HT-2 were obtained from the toluene/methanol mixture solvent with a methanol volume ratio of 90%.

Table S1. Solubility Parameters of Toluene, Methanol, Toluene/Methanol Mixtures, and Polystyrene and Deviations between the Solubility Parameters of Toluene/Methanol Mixtures and Polystyrene

V_{s1} (%)	V_{s2} (%)	δ_1 (J$^{1/2}$/cm$^{3/2}$)	δ_2 (J$^{1/2}$/cm$^{3/2}$)	δ_{mix}	δ_{PS} (J$^{1/2}$/cm$^{3/2}$)	$\Delta = \lvert \delta_{mix}-\delta_{PS} \rvert$
75	25	18.2	29.7	21.08	18.6	2.48
67	33	18.2	29.7	22.03	18.6	3.43
57	43	18.2	29.7	23.15	18.6	4.54
50	50	18.2	29.7	23.95	18.6	5.35
33	67	18.2	29.7	25.87	18.6	7.27
25	75	18.2	29.7	26.83	18.6	8.23
10	90	18.2	29.7	28.55	18.6	9.95

V_{s1}: Toluene volume ratios in the toluene/methanol mixtures.

V_{s2}: Methanol volume ratios in the toluene/methanol mixtures.

δ_1: Solubility parameter of toluene.

δ_2: Solubility parameter of methanol.

δ_{mix}: Solubility parameters of the toluene/methanol mixtures.

δ_{PS}: Solubility parameter of poly(styrene).

Δ: Deviations of δ_{mix} and δ_{PS}.

$\delta_{mix} = V_{s1}\delta_1 + V_{s2}\delta_2$